Progress in Nuclear Energy 116 (2019) 95–107

Contents lists available at ScienceDirect

Progress in Nuclear Energy

journal homepage: www.elsevier.com/locate/pnucene

Detailed neutronic calculations of the AP1000 reactor core with the Serpent code

Giovanni Laranjo de Stefani[a,b], João Manoel Losada Moreira[a,*], José Rubens Maiorino[a,c], Pedro Carlos Russo Rossi[a]

[a] CECS – Centro de Engenharia, Modelagem e Ciências Sociais, Universidade Federal do ABC, Av. dos Estados, 5001, 09210-580, Santo André, SP, Brazil
[b] Instituto De Pesquisas Energéticas E Nucleares, Ipen/Cnen-Sp, Av. Professor Lineu Prestes 2242, 05508-000, São Paulo, SP, Brazil
[c] DESTEC- Department of Energy, Systems, Territory, and Construction Engineering, Largo Lucio Lazzarino, 56122, Pisa, PI, Italy

A B S T R A C T

In this work we present some validation results for reactor core modeling with the Serpent code performed for the first cycle of the AP1000 reactor. The comparison with reported values of the assembly k_∞ for cold zero-power condition showed a discrepancy of 0.29%. The k_{ef} for full-core static and burnup calculations of the very heterogeneous AP1000 reactor core also presented good agreement with reported values. The k_{ef} for states with uniform fuel and moderator temperature distributions showed discrepancies below 0.91%. The boron worth curve obtained from burnup calculations with the Serpent code model results reproduced very well literature results despite using uniform temperature distributions in the modeling. In addition we discuss shadowing effects among burnable absorber rods (IFBA and Pyrex) and control rods which are, together with soluble boron, the control means throughout the first cycle. For instance, the presence of 9 Pyrex rods in an assembly decreased the average reactivity worth of one IFBA rod from 147 pcm to 33 pcm; and the presence of 28 IFBA rods in an assembly decreased the average reactivity worth of one Pyrex rod from 631 pcm to 277 pcm. The reactivity worth of a black control rod reduces about 20% when 28 IFBA rods are inserted in the fuel assembly.

1. Introduction

Recent advances in nuclear power generation aim to improve its economic competitiveness regarding the construction of nuclear power plants, efficient and safe operation and different indicators of sustainability (Moreira et al., 2013; Westinghouse, 2011; NEA, 2006; Moreira et al., 2015). The second goal requires that the core of advanced Pressurized Water Reactors (PWRs) have specifications such as long fuel cycles, low power densities and extensive use of burnable absorbers which require refined calculation to treat the fuel assembly heterogeneities. These studies require detailed physical modeling for assembly and full-core calculations and subsequent validation of the calculation methods. Examples of such studies coupled with method validation include the advanced PWR cores such as the AP1000 reactor (Franceschini et al., 2014; Souza and Moreira, 2006; Souza and Moreira, 2006a; Godfrey, 2014; Palmtag and Godfrey, 2014), advanced cores with different U−Pu or U−Th mixed fuels (Chambers and Ragusa, 2014; Alhaj et al., 2016; Baldova et al., 2014; Ernout et al., 2015; Lindley et al., 2014; Maiorino et al., 2017; Stefani, 2017).

A key problem of such core design calculations is related to the strong heterogeneities present in the fuel assembly. A good example of this is the core design for the AP1000 first cycle which includes as many as 112 burnable absorber rods of different designs within some of their 17 × 17 fuel assemblies (Westinghouse, 2011). This high number of absorber rods with short distances from each other creates important reactivity shadowing effects so that the combined reactivity worth of all of them together is quite different from the worth of the summation of individual absorber rods.

The main objective of this work is to present some verification and validation results performed for the first cycle of the AP1000 reactor core configuration using the Serpent code, a three-dimensional continuous-energy Monte Carlo particle transport code (Leppanen et al., 2015; Leppanen, 2015). The choice of this AP1000 core configuration is due to its advanced design featuring, fuel regions with important heterogeneities, a combination of two different burnable absorbers, different axial fuel enrichments and a low-leakage 18 month fuel cycle (Franceschini et al., 2015; Godfrey, 2014). The Serpent code, besides being available for general use, allows modeling of complex 3-dimensional geometries, uses ENDF/B-VII.0 cross-section library, has fuel depletion capability and has an efficient and fast running algorithm (Leppanen, 2015; Leppanen et al., 2015). In the validation process we pay special attention to the problem of reactivity shadowing effects among the burnable absorber rods present in the different AP1000 fuel assemblies. This is an important issue because the burnable absorbers

* Corresponding author. CECS – Centro de Engenharia, Modelagem e Ciências Sociais, Universidade Federal do ABC, Av. dos Estados, 5001, 09210-580, Santo André, SP, Brazil.
E-mail addresses: laranjogiovanni@gmail.com (G. Laranjo de Stefani), joao.moreira@ufabc.edu.br (J.M. Losada Moreira), joserubens.maiorino@ufabc.edu.br (J.R. Maiorino), pedro.rossi@ufabc.edu.br (P.C. Russo Rossi).

https://doi.org/10.1016/j.pnucene.2019.03.030
Received 5 March 2018; Received in revised form 23 February 2019; Accepted 17 March 2019

and soluble boron control its core excess reactivity throughout the first fuel cycle and the former, unquestionably, presents the most challenging modeling problems.

Although the AP1000 is a well-known and discussed nuclear power plant, collecting detailed information about it in the open literature is not a simple task. The information utilized in this work comes from the Westinghouse report about the AP1000 reactor design (Westinghouse, 2011), technical articles from the comprehensive VERA benchmark program (Godfrey, 2014; Franceschini et al., 2014; Palmtag and Godfrey, 2014) and other technical articles. We start presenting the data and methods with detail and follow with a section of results and discussions and finish with conclusions.

2. Reactor core data and calculation methods

We start collecting information in the open literature about AP1000 for performing detailed reactor physics calculations with the Serpent code. The parameters used for validating the calculation method and physical modeling are the k_∞ for unit cells and assemblies, k_{ef} for full core calculations, the fuel and moderator temperature coefficients, and the boron reactivity coefficient. Then we perform full core burnup calculations for the first 18 month cycle obtaining the boron worth curve, consumption of ^{235}U and ^{238}U and production of transuranic elements, ^{239}Pu and ^{241}Pu. To verify these results we compare them with those from the literature. We discuss the reactivity shadowing effects among the burnable absorbers in the AP1000 reactor core and, finally, present the conclusions.

2.1. General description of the AP1000

The material and geometric data describing the AP1000 reactor core were collected from available literature (Westinghouse, 2011), and reports from the VERA benchmark program (Franceschini et al., 2014; Godfrey, 2014; Palmtag, and Godfrey, 2014). The AP1000 advanced PWR reactor operates at a nominal power of 3400 MWt and contains 157 fuel assemblies with 3 different enrichment regions as shown in Fig. 1. Region 1 has fuel with ^{235}U enrichment of 4.45 w/o, region 2, of 3.40 w/o, and region 3 of 2.35 w/o. The fuel assembly contains a 17 × 17 matrix with 264 fuel rods and 25 guide tubes. The guide tubes can be used to insert instrumentation and burnable absorber rods. The beginning of cycle (BOC) core has two types of burnable absorbers: the Integral Fuel Burnable Absorber (IFBA) and the Pyrex Burnable Absorber. The IFBA rods occupy some of the positions of the fuel rods while the Pyrex rods occupy some of the guide tube positions. In Fig. 1, the number of IFBA rods present in a fuel assembly is indicated by the letter I and the number of Pyrex rods is indicated by the letter P (Westinghouse, 2011).

The detailed information about the ZrB_2 coating thickness in the IFBA and its specific mass were obtained from Walker (2014). Geometric and material data from the Pyrex burnable absorbers were obtained from Godfrey (2014). The variable axial distribution of ^{235}U enrichment in the IFBA burnable absorber rods were obtained from (Elsawi and Hraiz, 2015). Since the data describing the AP1000 fuel cells and assemblies were dispersed in many publications, the collected data used in this work are presented in Appendix A.

2.2. Calculation method

We use the Serpent code, a three-dimensional continuous-energy Monte Carlo particle transport code, developed for several purposes including reactor physics calculations encompassing fuel cell and assembly calculations, spatial homogenization, few energy-group cross-section generation, full core criticality calculations and fuel cycle studies (Leppanen et al., 2015; Leppanen, 2015). The Serpent code version we utilized has a cross-section library based on the ENDF/B.VII.0 data files with data at the following temperatures: 300 K, 600 K, 900 K, 1500 K and 1800 K. Although one finds in the literature thermal-hydraulic interfaces for the Serpent code (Kerby et al., 2017) we adopted flat temperature profiles for the fuel and moderator temperatures. In this study, no thermal-hydraulic feedback was used in the calculations to correct cross-sections due to variable fuel and moderator temperature distributions that occur at power conditions.

The calculations in the Serpent for determination of integral parameters such as k_{ef} were done using 200,000 histories and 2,000 cycles and for determination of differential quantities such as neutron flux and power density distribution, 4,000,000 histories and 2,000 cycles. The burnup calculations consider depletion zones for the assemblies of each fuel enrichment region with 50 axial divisions of 8.534 cm. The

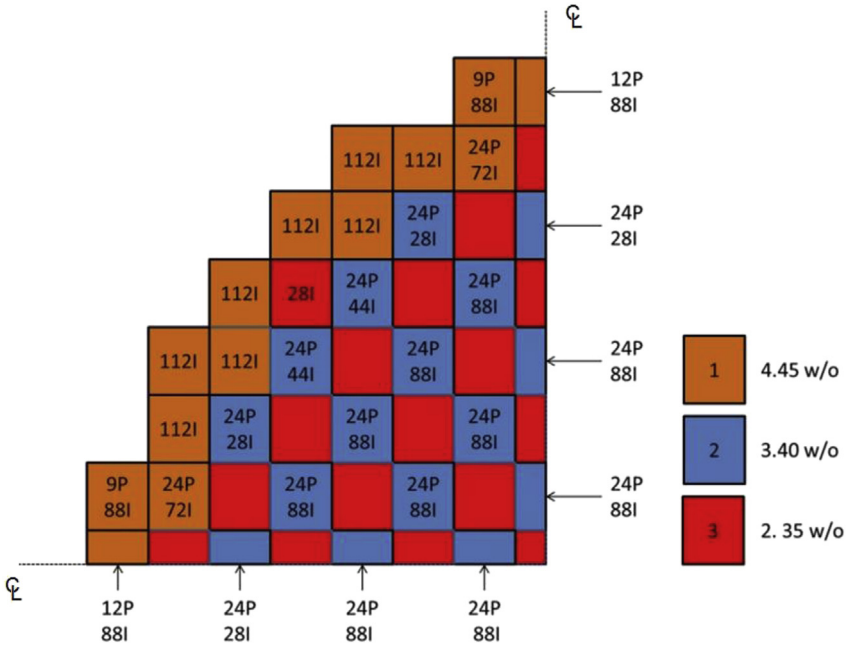

Fig. 1. AP1000 reactor core showing the 3 regions of different ^{235}U enrichments. The numbers indicate the amounts of burnable absorber rods of each type in a given fuel assembly: IFBA (I) and Pyrex (P); w/o means weight %.

depletion steps were 1 day for the first 7 days to account for xenon effects and 30 days for the remaining 450 days. To attain the curve of critical boron concentration we regarded that at the end of cycle it is zero. Thus the critical boron concentration is equal to that value which makes the k_{ef} at each time step equal to that of the end of cycle.

2.3. Data to verify calculations

The published data about neutronic calculations used to verify this work's results are mostly based on Chapter 4 of the AP1000 reactor report available in the US Nuclear Regulatory Commission site (Westinghouse, 2011; Maiorino et al., 2017). This report presents results for infinite and effective multiplication factors for different assembly and full core configurations, burnup results for the first reactor core, temperature coefficients of reactivity and soluble boron coefficient of reactivity. The VERA core physics benchmark program provides neutronic results for several AP1000 parameters and are also utilized (Godfrey, 2014).

2.4. Three-dimensional full-core model of the AP1000 with the serpent code

The core temperatures at cold and hot zero-power isothermal states were based on Westinghouse (2011). The core temperature at full power (3400 MWt) and specific mass were taken from Godfrey (2014). Table 1 identifies the conditions describing the 3 core states considered in this work: cold zero-power (CZP), hot zero-power (HZP) and hot full-power (HFP). It presents for each reactor state the fuel temperature, structure (including clad) and moderator temperatures, the moderator specific mass, temperature for S(α,β) treatment for binding effects on the moderator cross-sections, and temperatures considered in the Serpent code cross-section library (Viitanen and Leppänen, 2012). The temperatures considered for the S(α,β) treatment data are the closest available in the Serpent code cross-section library to those of the actual AP1000 reactor states (Leppanen et al., 2015; Leppanen, 2015). The temperatures in Table 1 were adjusted by Doppler-broadening.

Table 2 presents the AP1000 configurations considered in this work for calculations of fuel cell, fuel assembly and reactor core. These configurations include different fuel enrichment levels, soluble boron concentration in the coolant, 2 types of burnable absorbers and reactor core conditions. As indicated in Fig. 1, the number and configuration of burnable absorber rods differ from one assembly to another and are described with detail in section A4 of Appendix A.

2.5. Temperature coefficients of reactivity

To calculate the temperature coefficients of reactivity we considered the core conditions presented in Table 1. The fuel temperature coefficient of reactivity was calculated for fuel temperature varying between 600 K and 1800 K, with 300 K intervals setting the temperature of the other materials to 600 K.

The moderator temperature coefficient of reactivity was calculated by setting all materials to the temperatures of 600 K. To correct the moderator cross-sections with temperature, we varied the S(α,β) treatment temperature and the water specific mass in accordance with the moderator temperature varying between 300 K and 600 K in 50 K intervals.

Each fuel or moderator temperature condition configured a different state. The reactivity change due to the variation of temperature was associated to the reactivity change between these states and was obtained from

$$\Delta\rho = \frac{k_2 - k_1}{k_2 k_1} \quad (pcm) \tag{1}$$

where k_1 and k_2 are the effective multiplication factor furnished by the Serpent code for temperature states 1 and 2, respectively, and pcm means 10^{-5}.

2.6. Reactivity of control rods, burnable absorbers and shadowing effects

The reactivity effects of control rods and the burnable absorbers are studied through fuel assembly calculations. They were modeled in three-dimensional geometry applying total reflection boundary conditions at the X−Y boundaries and a 30 cm water reflector at the top and bottom ends of the assembly (Z direction). The two burnable absorbers, IFBA and Pyrex, are considered and several assembly states with different number of IFBA and Pyrex absorber rods are constructed, as shown in Table 2. Figures A5 and A6 from Appendix A show the location of the burnable absorbers in the fuel assemblies. As the number of burnable absorber rods increase the distances among them are reduced as shown in Fig. A5. The control rod inserted in the assembly refers to the black control bank (Westinghouse, 2011).

Reactivity shadowing occurs due to the proximity of absorbing rods with one another. In the AP1000 core there are fuel assemblies with different configurations of burnable absorber rods of the Pyrex and IFBA types and their number varies from 112 to 28 absorber rods and as shown in Fig. 1. The IFBA rods are mostly concentrated in the central part of the assembly near the location of the absorber rods of the control element and the Pyrex rods are located in the positions of the control element rods. As the number of burnable absorber rods increases in the fuel assembly they are positioned very close to one another and thus undergo reactivity shadowing effects. For instance, the average distance between IFBA rods in the 28 I configuration is approximately 3.44 pitches in the central part of the fuel assembly while in the 112 I configuration it is approximately 1.35 pitches (see Figure A5). Thus the reactivity effectiveness of the burnable absorbing rods or a control element depends on the number and configuration of burnable absorber rods in the assembly.

To calculate the reactivity introduced by burnable absorbers and determine possible rod shadowing effects we used Eq. (1) and perturbation theory (Bell and Glasstone, 1970). Considering a given configuration of Table 2 and calling it state 1, an additional quantity of burnable absorber added to this state is considered a perturbation which defines a state 2. The reactivity due to this additional quantity of burnable absorber in the assembly at state 1 is given by Eq. (1) with

Table 1
Description of the three core states considered in the Serpent model of this work.

Reactor state	Fuel temperature (K)	Moderator and structure temperature (K)	Moderator specific mass (g/cm³)[a]	Temperature for S(α,β)[b] (K)	Temperature in the cross-section library (K)
CZP - cold zero-power	293.6	293.6	0.995	293.6	300[b]
HZP – hot zero-power	565	565	0.744	550	565
HFP – Hot full-power[c]	900	565	0.744	550	900 (fuel) and 565 (moderator and structures)

[a] Considering pressure of 1 atm for CZP and of 153 atm for HZP and HFP.
[b] Closest temperatures available in the Serpent code.
[c] Full power: 3400 MWt

Table 2
AP1000 configurations or states considered in this work for calculations of fuel cell, fuel assembly and full-core.

Configuration or state[a]	Description	Type of calculation
R1.58	Fuel cell with 1.58 w/o^{235}U enrichment and at CZP	Cell
R2.35	Fuel cell with 2.35 w/o^{235}U enrichment and at CZP	Cell
R3.20	Fuel cell with 3.20 w/o^{235}U enrichment and at CZP	Cell
R3.40	Fuel cell with 3.40 w/o^{235}U enrichment and at CZP	Cell
R4.45	Fuel cell with 4.45 w/o^{235}U enrichment and at CZP	Cell
A2.35 + 9P	Assembly 17 × 17, CZP, BOC, water without soluble boron, 9 Pyrex rods and 2.35 w/o^{235}U enrichment.	Assembly
A2.35 + 9P + 28I	Assembly 17 × 17, CZP, BOC, non-borated water, 9 Pyrex rods, 28 rods with IFBA and 2.35 w/o^{235}U enrichment.	Assembly
A2.35	Assembly 17 × 17, CZP, BOC, water without soluble boron and 2.35 w/o^{235}U enrichment.	Assembly
A2.35 + 28I	Assembly 17 × 17, CZP, BOC, water without soluble boron, 2.35 w/o^{235}U enrichment and 28 rods with IFBA.	Assembly
A3.40 + 24P + 28I	Assembly 17 × 17, CZP, BOC, water without soluble boron, 3.40 w/o^{235}U, 24 Pyrex rods and 28 IFBA rods.	Assembly
A3.40 + 24P + 44I	Assembly 17 × 17, CZP, BOC, water without soluble boron, 3.40 w/o^{235}U, 24 Pyrex rods and 44 rods with IFBA.	Assembly
A3.40 + 24P + 88I	Assembly 17 × 17, CZP BOC, water without soluble boron, 3.40 w/o^{235}U, 24 Pyrex rods and 88 rods with IFBA.	Assembly
A4.45 + 9P + 88I	Assembly 17 × 17, CZP, BOC, water without soluble boron, 4.45 w/o^{235}U, 9 Pyrex rods and 88 rods with IFBA.	Assembly
A4.45 + 24P + 72I	Assembly 17 × 17, CZP, BOC, water without soluble boron, 4.45 w/o^{235}U, 24 Pyrex rods and 72 rods with IFBA.	Assembly
A4.45 + 12P + 88I	Assembly 17 × 17, CZP, BOC, water without soluble boron, 4.45 w/o^{235}U, 12 Pyrex rods and 88 rods with IFBA.	Assembly
A4.45 + 112I	Assembly 17 × 17, CZP, BOC, water without soluble boron, 4.45 w/o^{235}U and 112 rods with IFBA.	Assembly
C-CZP	Full core, CZP, BOC, water without soluble boron and control banks removed.	Core
C-CZP + B1574	Full core, CZP, BOC, water with soluble boron (1574 ppm) and control banks removed.	Core
C-HZP	Full core, HZP, BOC, water without soluble boron and control banks removed.	Core
C-HZP + B1382	Full core, HZP, BOC, water with soluble boron (1382 ppm) and control rods removed.	Core
C-HZP + B1502	Full core, HZP, BOC, water with soluble boron (1502 ppm) and control banks removed.	Core
C−HFP + B1184	Full core, HFP, BOC, without xenon, water with soluble boron (1184 ppm) and control banks removed.	Core
C−HFP + B827 + XE	Full core, HFP, BOC, xenon equilibrium, water with soluble boron (827 ppm) and control banks removed.	Core
C−HFP	Full core, HFP, BOC, water not bored and control banks removed.	Core

[a] The letters R, A and C in the configuration names stand for cell calculation, assembly calculation and three-dimensional core calculation.

states 1 and 2 now defined in terms of number of burnable absorber rods or the presence of control rods. The average reactivity insertion of one burnable absorber rod is obtained by dividing these results by the number of additional rods introduced in state 1.

In all IFBA rods the fuel enrichment at the ends changes from 1.58 w/o to 3.2 w/o (see Appendix A). Thus the IFBA rods promote two effects on the core: reactivity decrease due to neutron absorption by the ZrB_2 coating and reactivity increase due to higher enrichment at their ends. These two effects must be taken into account to infer correctly the reactivity insertion of such burnable absorber rods into the AP1000 reactor core. The net effect is influenced by the shadowing effects discussed above.

3. Serpent code results and discussions

3.1. Verification of assembly and full core calculations

Table 3 presents the comparison between the infinite multiplication factor and effective multiplication factors obtained in this work with those from Westinghouse (2011). The AP1000 core states are at beginning of cycle CZP and HZP conditions, different soluble boron concentrations as described in Table 2. We have considered data from Westinghouse (2011) presenting 2 and 3 significant digits after the decimal point. To estimate the discrepancy we have assumed an uncertainty of ± 0.005 and ± 0.0005 for the data with 2 and 3 significant digits, respectively. The discrepancies are presented in ranges of maximum and minimum values.

Table 3
Effective multiplication factor for different core configurations compared to Westinghouse results.

Configuration or state	k_{ef} (This work)	k_{ef} Westinghouse (2011)	Discrepancy range (%)
A-2.35	1.33112 ± 0.00008[a]	1.328[a]	(0.20, 0.27)
C-CZP	1.20201 ± 0.00004	1.205	(-0.29, −0.21)
C-CZP + B1574	0.99398 ± 0.00004	0.99	(-0.10, 0.91)
C-HZP + B1502	0.99188 ± 0.00004	0.99	(-0.31, 0.70)

[a] This result is k_∞.

The comparison in Table 3 of the assembly k_∞ calculation for CZP condition shows a reasonable agreement. The maximum discrepancy of −0.29% can be associated to the different cross-section libraries since this work uses the ENDF/B.VII.0 library while in the report is used the ENDF/B.V library.

The comparison in Table 3 of effective multiplication factors for full core at CZP and HZP condition show acceptable agreement (< 0.91%). The possible reasons for this discrepancy are similar to those discussed above for the assembly calculation and possibly the modeling of the burnable absorber rods, especially the IFBA. The addition of soluble boron increased slightly the discrepancy.

From these comparisons we can conclude that current model of the AP1000 code with the Serpent code yields effective multiplication factors that reproduce published results with discrepancy below 0.91%. The approximations for fuel and moderator temperatures and the IFBA burnable absorber models adopted in this work appear adequate for CZP and HZP conditions. No thermal-hydraulic feedback was used in the calculations. The HFP conditions were approximated with uniform temperature distributions.

3.2. Fuel cell calculations

We present in Fig. 2 the k_∞ and respective standard deviation for the fuel cells appearing in the AP1000 assemblies and described in Table 2 and in Appendix A. The Monte Carlo calculations with the Serpent code present standard deviations smaller than 4 pcm.

The results shown in Fig. 2 allow assessing the influence of enrichment on the core reactivity. The k_∞ presents a declining derivative with respect to the enrichment indicating that to obtain higher k_∞ to obtain longer fuel cycles, for example, it would be necessary important increases in fuel enrichment.

3.3. Fuel assembly calculations and reactivity shadowing effects among the burnable absorber rods

Table 4 presents the k_∞ and the respective standard deviation for the several assembly configurations described in Table 2 and in Appendix A, sect. A4, Figures A5 and A6. In these calculations, the fuel

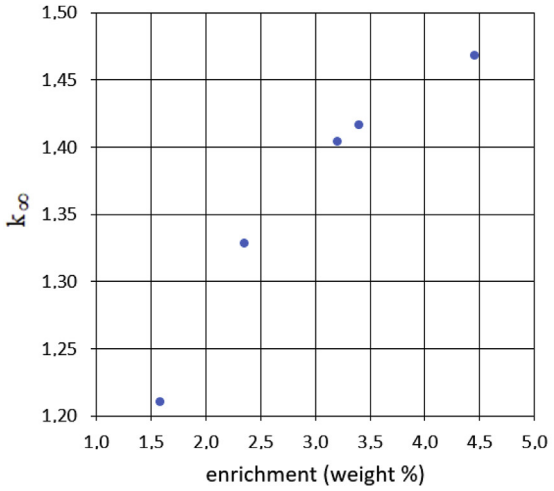

(a)

Config.	k_∞
R1.58	1.21029 ± 0.00003
R2.35	1.32863 ± 0.00004
R3.20	1.40462 ± 0.00004
R3.40	1.41697 ± 0.00004
R4.45	1.46858 ± 0.00003

(b)

Fig. 2. (a) Fuel cell k_∞ as a function of the enrichment for different configurations described in Appendix A. The uncertainties are too small to appear in the figure and are presented in the box at the right (b) together with the k_∞ values.

assemblies were modeled as described in Sect. 2.6.

In Table 5 we present results of shadowing effects in the control element burnable absorbers due to the presence of other absorber rods in the fuel assembly. The assembly considered is the A2.35 (see Table 2) and the reactivity changes are obtained as described in Sect. 2.6. To estimate the rod shadowing effect of 28 IFBA rods on the reactivity worth of the control rod we considered the states A2.35 and A2.35 + CR (without burnable absorber) and A2.35 + 28I and A2.35 + 28I + CR (with burnable absorber). The control rod worth decreased 50% due to the presence of 28 IFBA rods in the assembly. Table 5 also attempts to compare the reactivity worth of IFBA and Pyrex burnable absorbers in the fuel assembly and to infer the shadowing effect caused on their reactivity worth due to the presence of other absorbers in the assembly. The reactivity from the IFBA absorbers is taken as the change of reactivity between configurations or states A2.35 + 28I and A2.35; the reactivity from the Pyrex absorbers is taken as the change of reactivity and between configurations A2.35 + 9P and A2.35. The average reactivity insertion of one rod is obtained by dividing these results by the number of rods in these configurations, 28 and 9 for the IFBA and Pyrex burnable absorbers, respectively.

To obtain the average reactivity of one burnable absorber rod shadowed by other absorber rods present in the assembly we followed a similar approach. For the IFBA rods shadowed by 9 Pyrex rods, we obtained it from the reactivity change between configurations A2.35 + 9P and A2.35 + 9P + 28I divided by 28. Conversely, for the Pyrex rods shadowed by 28 IFBA we obtained it from the reactivity change between configurations A2.35 + 28I and A2.35 + 9P + 28I divided by 9. For the Pyrex rods shadowed by 88 IFBA and 9 Pyrex rods we considered the reactivity change between configurations A4.45 + 9P + 88I and A4.45 + 12P + 88I divided by 3.

Fig. 3 presents the k_∞ as a function of the number of IFBA burnable absorber rods in the assembly and shows the saturation effect that the

Table 5
Observed reactivity effects of IFBA and Pyrex burnable absorber rods in the A2.35 fuel assembly.

Description	Reactivity (pcm)
Control bank worth for the A2.35 assembly configuration	12453
Control bank worth for the A2.35 assembly configuration with 28 IFBA rods	6216
Reactivity due to 28 IFBA inserted into the A2.35 assembly configuration	4117
Reactivity due to 9 Pyrex burnable absorbers inserted in the A2.35 configuration	5679
Average reactivity of one IFBA rod	147
Average reactivity of one Pyrex burnable absorber rod	631
Average reactivity of one IFBA rod shadowed by 9 Pyrex rods	33
Average reactivity of one Pyrex rod shadowed by 28 IFBA rods	277
Average reactivity of one Pyrex rod shadowed by 88 IFBA + 9 Pyrex rods	67

Table 4
Assembly k_∞ and respective standard deviation for several assembly configurations for the AP1000 power reactor. The configurations are described in Table 2.

Configuration	k_∞ (3-D)	Enrichment (weight %)	Burnable Absorber rods		Control banks
			Pyrex	IFBA	
A2.35	1.33112 ± 0.00008	2.35	0	0	Removed
A2.35 + 28I	1.26197 ± 0.00008	2.35	0	28	Removed
A2.35 + 9P	1.23757 ± 0.00008	2.35	9	0	Removed
A2.35 + 9P + 28I	1.22352 ± 0.00008	2.35	9	28	Removed
A2.35 + CR	1.14184 ± 0.00008	2.35	0	0	Inserted
A2.35 + 28I + CR	1.17018 ± 0.00008	2.35	0	28	Inserted
A3.40 + 24P + 28I	1.26895 ± 0.00008	3.40	24	28	Removed
A3.40 + 24P + 44I	1.23642 ± 0.00008	3.40	24	44	Removed
A3.40 + 24P + 88I	1.22529 ± 0.00008	3.40	24	88	Removed
A4.45 + 9P + 88I	1.28804 ± 0.00008	4.45	9	88	Removed
A4.45 + 12P + 88I	1.28473 ± 0.00008	4.45	12	88	Removed
A4.45 + 24P + 72I	1.26524 ± 0.00008	4.45	24	72	Removed
A4.45 + 112I	1.30754 ± 0.00008	4.45	0	112	Removed

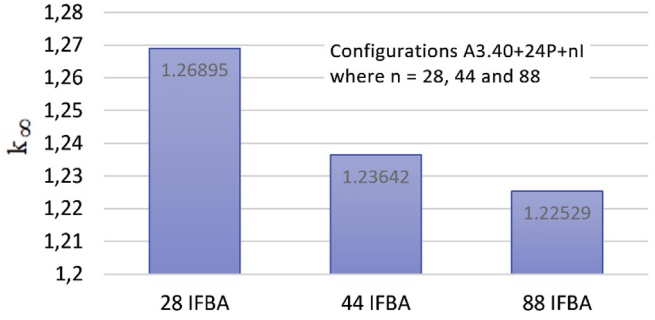

Fig. 3. Infinite multiplication factor for configuration A3.40 + 24P + 28I, A3.40 + 24P + 44 and A3.40 + 24P + 88I showing the decreasing impact of the number of burnable absorber rods due to shadowing effects.

burnable absorber rods experience as their number in the assembly is increased.

These assembly calculations allow us to analyze several effects of the reactivity control means available in the AP1000 reactor core. The reactivity insertion by Pyrex burnable absorber rods is greater than that by IFBA rods. While 28 IFBA rods inserted 4117 pcm into the A2.35 assembly, 9 Pyrex rods inserted 5679 pcm. The average inserted reactivity by a Pyrex rod is about 4 times greater than that by an IFBA rod.

The reactivity shadowing effects among control rods, IFBA rods and Pyrex rods are very important. Table 5 attempted to account the shadowing effects between IFBA and Pyrex rods in the A2.35 assembly configuration. The average reactivity worth of one IFBA rod in the 28 I configuration decreased from 147 pcm to 33 pcm when 9 Pyrex rods were inserted into the assembly. Similarly, the average reactivity worth of one Pyrex rod in the 9P configuration decreased from 631 pcm to 277 pcm when 28 IFBA rods were inserted into the assembly and to 67 pcm when 88 IFBA plus 9 Pyrex rods were inserted into the assembly. These results show that the shadowing effects are very strong. Accurate calculations of such a heterogeneous assembly require at least detailed two-dimensional transport approach in the assembly level.

This result is corroborated by Fig. 3 where one sees that as the number of IFBA rods increases the rate of decrease in the k_∞ is reduced due to growing shadowing effects. The assembly configuration with 88 IFBA and 24 Pyrex has 112 burnable absorber rods positioned very close to each other as can be seen in Figure A5 (the Pyrex rods occupy the control rod positions). The small distances between the burnable absorber rods cause important shadowing effect. Fig. 3 shows also that beyond 80 or 90 IFBA rods in the assembly there is no important increase in the on the neutron absorption, i.e., more absorber rods will produce negligible impact on the assembly reactivity.

Comparing the k_∞ for assembly configurations A2.35 + CR and A2.35 + 28I + CR we note that adding the 28 IFBA burnable absorber rods actually increased the assembly k_∞. One would expect the k_∞ for configuration A2.35 + 28I + CR to be lower than that of A2.35 + CR but not very much due to shadowing effects among control and IFBA rods in the assembly. The higher k_∞ shown in Table 5 for configuration A2.35 + 28I + CR is due to the higher ^{235}U enrichment at the top and bottom ends of the IFBA rods.

This effect has impact on the worth of individual control rods. The combined effect of adding absorption through ZrB_2 coating on the fuel rods (insertion of IFBA rods) and increasing ^{235}U enrichment at the fuel rod ends is a net decrease of about 20% in control rod worth (see Table 5).

3.4. Results from full core calculations and discussion

Table 6 presents the comparison of the neutron flux for different energy ranges between results from this work and from Westinghouse (2011) for HFP conditions. The average and peak power densities are also presented in Table 6 and the latter is compared to the Westinghouse (2011) results. Figs. 4 and 5 show the neutron flux distribution on horizontal and vertical planes (X−Y and Y-Z) for thermal and epithermal energies (E < 5.53 keV). Fig. 6 shows the power density distribution in the X−Y plane at the mid height (Z axis). The figure presents results for each rod position and the yellow dots are located on guide tube positions. In all figures the reactor power level is 3400 MW.

Table 6
Neutron flux at the center of the reactor core for C−HFP.

Energy range	Neutron flux (this work)	Neutron flux Literature[a]
E ≥ 1.0 MeV	$1.37 \times 10^{14} \pm 0.09 \times 10^{14}$	1.12×10^{14}
5.53 keV < E < 1 MeV	$1.93 \times 1014 \pm 0.09 \times 1014$	1.76×1014
0.625 eV ≤ E < 5.53 keV	$1.18 \times 10^{14} \pm 0.13 \times 10^{14}$	1.28×10^{14}
E ≤ 0.625 eV	$5.01 \times 10^{13} \pm 0.21 \times 10^{13}$	5.47×10^{13}
Average power density (W/cm^3)	110.6	
	This work	**Literature[a]**
Power peak factor	2.71	2.60
Peak power density (W/cm^3)	299.73	287.56

[a] (Westinghouse, 2011).

The comparisons in Table 6 between the neutron flux from this work and those from Westinghouse (2011) show results for the four energy ranges in the core center outside the Monte Carlo uncertainties. This was expected since the model used in this work adopts uniform fuel and moderator temperatures for HFP conditions. In addition, three-dimensional burnup calculations for pressurized water reactors using the Monte Carlo methods are subject to spatial instabilities. Despite these problems the discrepancy at BOC for the power peak factor was 3.8%. In addition, such discrepancy is smaller than those from measured power density distribution with sophisticate monitoring schemes (Souza and Moreira, 2006; Souza and Moreira, 2006a).

3.5. Coefficients of reactivity

The fuel and moderator temperature coefficients of reactivity, α_F and α_M, and the soluble boron coefficient of reactivity, α_B, are presented in Table 7. These coefficients of reactivity were obtained as described in sect. 2.7 considering k_{ef} results from the configurations shown in Table 2 and their respective temperatures and boron concentration.

Table 7 shows that the results obtained in this work are in good agreement with those from Westinghouse (2011); the intervals covered for all 3 parameters are similar.

3.6. Calculations of reactivity control means and isotopic inventory as a function of burnup

The core reactivity control along the life cycle is performed through the burnable absorber rods and soluble boron. As explained in sect. 2.2, the curve of soluble boron worth presents the amount of boron to be diluted in the moderator so that the poisoned core k_{ef} at a given burnup level is the same as that at the end of the cycle. Fig. 7 compares for HFP condition the result of soluble boron worth curve obtained in this work with that furnished by Westinghouse (2011). The data was extracted from Westinghouse (2011) with the digitalization software (Huwaldt, 2015). Comparison of these 2 curves provides an overall verification of calculation methods regarding core reactivity and burnup since it includes fuel, moderator and reactivity control means through 2 types of burnable absorbers and soluble boron during the first cycle. The curves are almost superimposed.

Fig. 8 compares the isotope inventories of uranium and plutonium as a function of burnup between this work and the Westinghouse (2011). The power density considered was 123.3 W/cm^3 or 40.2 kW/kg U. The isotopes are ^{235}U, ^{238}U, ^{239}Pu and ^{241}Pu. The colored lines are

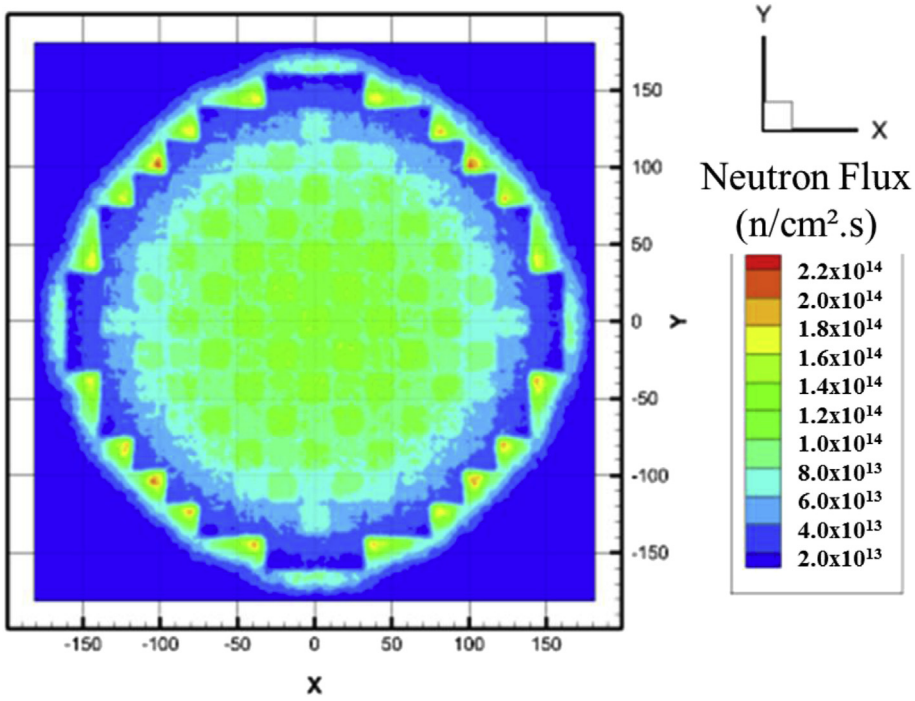

Fig. 4. Neutron flux (E < 5.53 keV) distribution (X−Y plane) for the C−HFP configuration. The z axis position is the center of the core. The reactor power level is 3400 MW.

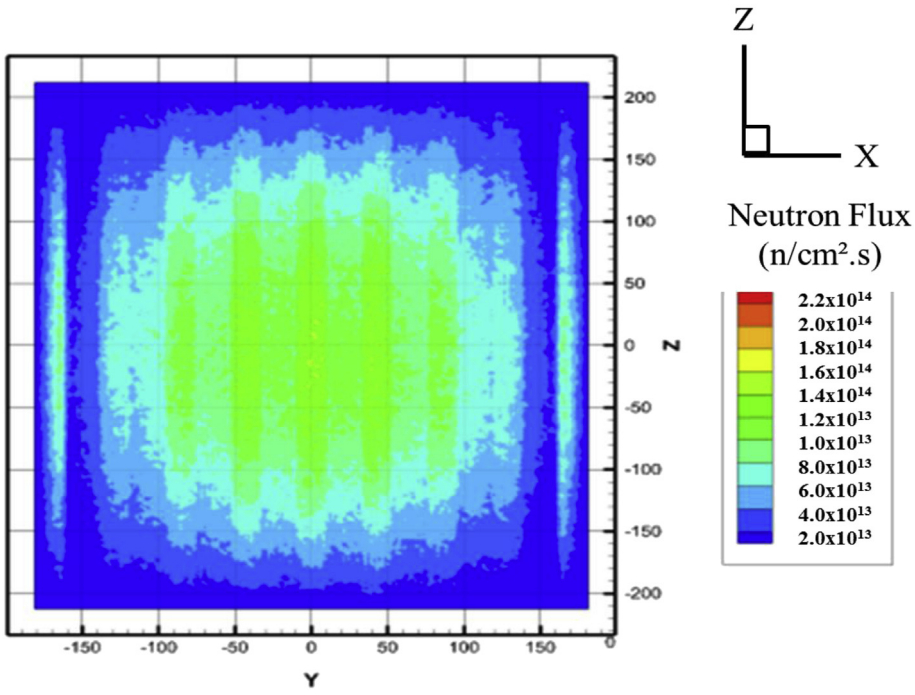

Fig. 5. Neutron flux (E < 5.53 keV) distribution (Y-Z plane) for the C−HFP configuration. The x axis position is the center of the reactor. The reactor. Power level is 3400 MW.

the results obtained in this work and the black lines are results from Westinghouse (2011) obtained through the digitalization software (Huwaldt, 2015). The maximum discrepancies occurred for ^{239}Pu, ^{235}U and ^{238}U and are presented in the figure legend. For other isotopes the results reproduce well the Westinghouse results.

Integral parameters such as k_{ef} or critical boron concentration calculated with Monte Carlo Methods do not present instabilities observed in differential results such as neutron flux and power density distributions. The good results presented in Fig. 7 shows that a calculation with the Serpent code using spatially averaged quantities such as burnup estimated in depletion zones and core average fuel and moderator temperatures reproduces the correct boron curve.

The boron worth curve allows some validation of the burnable absorber modeling for the IFBA adopted in this work (Walker, 2014), especially the ZrB_2 coating thickness. The good comparison indicates good modeling of the combined effects of core reactivity and of the control means throughout the first cycle. The subtle differences are considered due to different cross-section libraries, and the uniform fuel

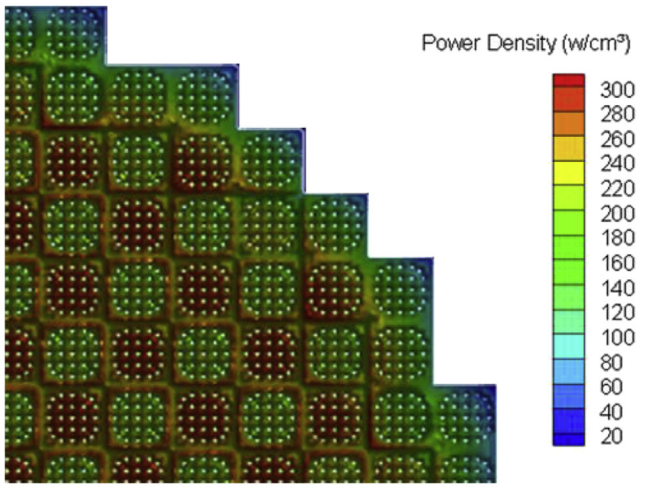

Fig. 6. Power density distribution for configuration C−HFP taken at the z axis position in the core center, the plane with maximum power density. The average and maximum core power densities are 110.6 W/cm^3 and 299.7 W/cm^3, respectively.

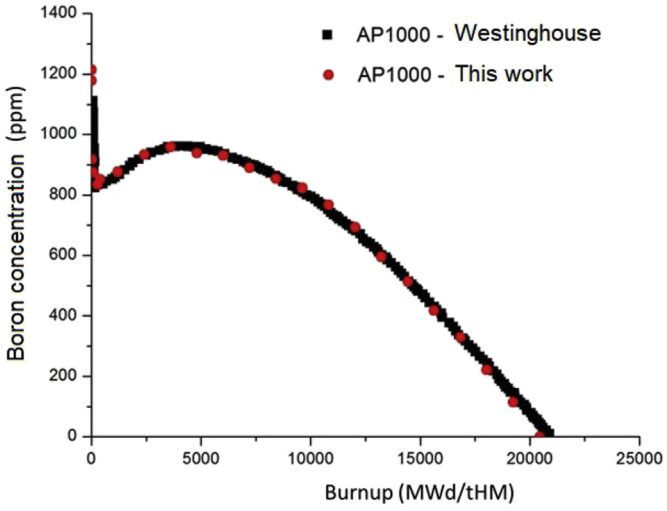

Fig. 7. Boron concentration in the moderator as a function of burnup (Curve of soluble boron worth). Comparison between results of this work and those from Westinghouse (2011).

and moderator temperature distribution approach adopted in this work for full power conditions.

The impact of different cross-section library data is clearly seen in Fig. 8 regarding the ^{239}Pu production and consumption of ^{235}U and ^{238}U. The discrepancy regarding ^{239}Pu disappears for high burnup levels, close to 40 GWD/MTU, while the discrepancy regarding ^{235}U and ^{238}U consumption increases for high burnup levels. Regarding the ^{239}Pu isotope production, the differences along the cycle appear to be due to simplifications in the decay chains. Regarding the consumption of ^{238}U and ^{235}U the differences are related to reaction rates. In this case the differences must be due to different cross-section libraries and the uniform fuel and moderator coolant distribution approximation for the HFP condition.

Observing the results of Figs. 7 and 8, one can conclude that the current model is accurate regarding core reactivity results. The good comparison of boron concentration in the coolant throughout the first cycle evidences that. For isotope estimation, differences around 5% at the end of the first cycle must be expected.

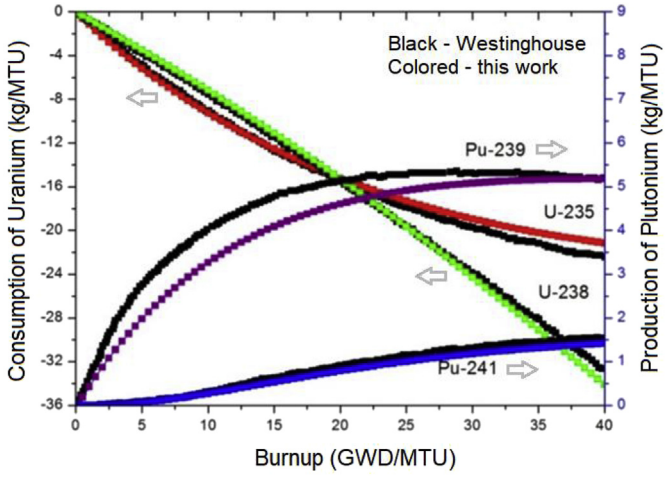

Fig. 8. Uranium consumption and Plutonium production as a function of burnup for the assembly configuration A1. Comparison between results from this work. and from Westinghouse (2011). Maximum discrepancies are −15% for ^{239}Pu, +4,4% for ^{238}U and −5,3% for ^{235}U.

4. Conclusions

The model presented in this work, with spatially average quantities regarding burnup and fuel and moderator temperatures, reproduces well results of the AP1000 reactor core for k_∞, k_{ef} and the critical boron concentration. The comparison with reported values of the assembly k_∞ for cold zero-power condition showed a discrepancy of 0.29%. The k_{ef} for full-core calculations of the very heterogeneous AP1000 reactor core also presented good agreement with reported values. The discrepancies for calculations at cold zero-power and hot zero-power conditions, which present uniform fuel and moderator temperature distributions, showed discrepancies below 0.91%. The burnable absorber models adopted in this work, especially the one for the IFBA, appear adequate to furnish results with this level of accuracy.

The results obtained for the fuel and moderator temperature coefficients of reactivity reproduced well the reported results for the AP1000 reactor core as well the boron coefficient of reactivity.

The assembly calculations allowed us to analyze the reactivity effects of the Pyrex and IFBA burnable absorbers and the strong shadowing in the heterogeneous assemblies of the AP1000 first cycle core. The average reactivity inserted by a Pyrex burnable absorber rod is about 4 times greater than that by an IFBA. The reactivity shadowing effect of these burnable absorber rods on each other in the assembly is

Table 7
Fuel and moderator temperature coefficients of reactivity and soluble boron coefficient of reactivity[a].

Temperature coefficient of reactivity	This work	Westinghouse (2011)
α_F(pcm/°F)	−2.87 ± 0.14 to −0.91 ± 0.14	−3.5 to −1.0
α_M(pcm/°F)	−3.72 ± 0.47 to −28.06 ± 0.53	0 to −35
α_B(pcm/ppm B)[b]	−11.32 ± 0.50 to −6.23 ± 0.50	−13.5 to −5.0

[a] Configurations defined in Table 2.
[b] ppm B – ppm of soluble boron in the reactor coolant.

very strong. For instance, the presence of 9 Pyrex rods in an assembly decreased the average reactivity worth of one IFBA rod from 147 pcm to 33 pcm; and the presence of 28 IFBA rods in an assembly decreased the average reactivity worth of one Pyrex rod from 631 pcm to 277 pcm. These results show that the shadowing effects are very strong. Accurate calculations of such a heterogeneous assembly require at least detailed two-dimensional transport approach in the assembly level.

Interesting reactivity shadowing effect among burnable absorbers and control rod were noticed in the AP1000 first cycle core. The fuel assembly k_∞ almost stabilizes (does not reduce) when more than 80 IFBA rods are inserted. The reactivity worth of a black control rod reduces about 20% when 28 IFBA rods are inserted in it.

The boron worth curve obtained in this work was almost coincident with the reported one despite the approximation of uniform temperatures for calculations at power conditions and depletion zones for burnup estimation. This curve provides an important overall validation of the Serpent model used in this work since they are three-dimensional full core calculations including all control means available in the AP1000 reactor core. In particular it indicates the good results yielded by the IFBA modeling adopted in this work.

The results show that this Serpent code model can be used to design studies of very heterogeneous reactor cores such as the AP1000 reactor. They evidence that calculations with the Serpent code using spatially averaged values for temperature and burnup reproduce well the boron curve, the reactivity of burnable poisons and other core integral parameters.

Acknowledgements

GLS and JMLM thank CAPES (Coordenação de Aperfeiçoamento de Pessoal de Nível Superior) for financing this work. JRM expresses his gratitude to DESTEC - University of Pisa and to Prof. Francesco D'Auria for his collaborative work. In addition the authors want to acknowledge the very helpful comments provided by the reviewers.

Appendix B. Supplementary data

Supplementary data to this article can be found online at https://doi.org/10.1016/j.pnucene.2019.03.030.

Appendix A

We present here the details of the data and materials of fuel rods and fuel assemblies of the AP1000 reactor. Whenever the data is not from Westinghouse (2011) their origin references are presented.

A1. Fuel cell and assembly geometric data

Fig. A1(a) shows a cross section of the fuel rod used in the fuel assembly and shows the dimensions of the fuel pellet, gap, Zirlo coating and the pitch and Fig. A1(b) shows the data describing the fuel rod. The distribution of fuel rods and guide tubes of a fuel assembly is shown in Fig. A2. This figure also shows the axial enrichment distribution in the fuel rod which at its ends is lower.

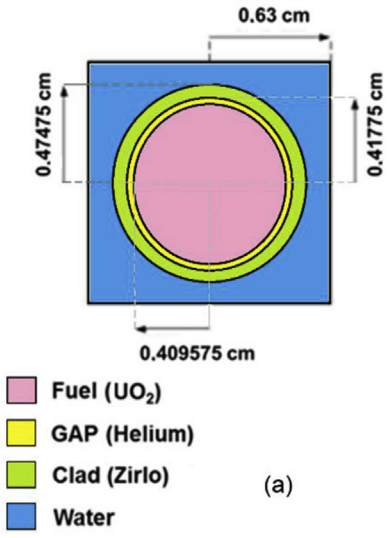

Parameter	Value
Fuel diameter*	0.81915 cm
Outside diameter*	0.94996 cm
Gap thickness*	0.01651 cm
Clad thickness*	0.05715 cm
Clad (Zirlo) specific mass**	6.56 g/cm³
Fuel (UO_2) specific mass†	95.5 % of theoretical
Gap (He) specific mass 300 K (1 atm)*** 565 K (153 atm)***	 1.62520×10^{-04} g/cm³ 1.2049×10^{-02} g/cm³
Fuel rod length*	426.72 cm
Pitch*	1.26 cm
Rod Array*	17x17
Fuel rods per assembly*	264
Water specific mass 300 K (1 atm) *** 565 K (153 atm) ***	 0.9980 g/cm³ 0.7441 g/cm³

* (Westinghouse, 2011)
** (Rajasekhara et al., 2017)
*** (NIST, 2017)
† (Popov et al., 2000)

(b)

Fig. A1. Schematic showing the dimensions and other data for the fuel rod including, gap, Zirlo clad and pitch.

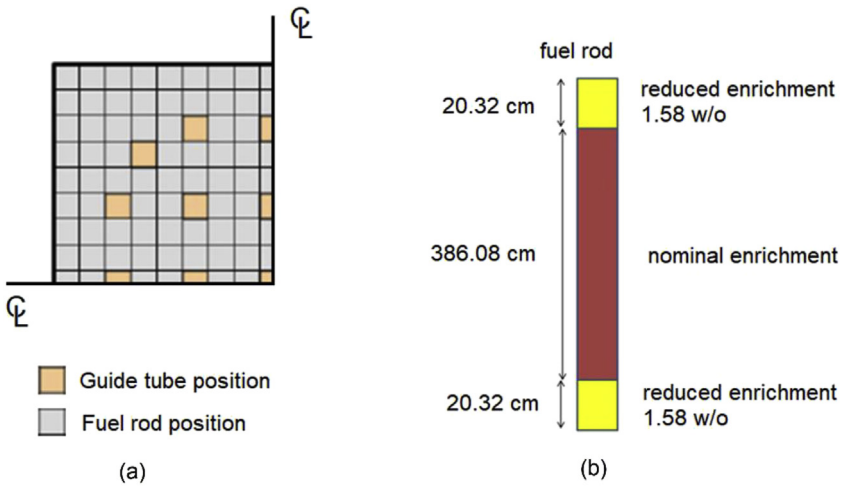

Fig. A2. Configuration of the fuel rods and guide tubes in fuel assembly (17 × 17) – left side (a) and axial fuel enrichment distribution for the AP1000 core – right side (b).2

The Zirlo data for the fuel clad demanded some literature survey. The clad alloy data adopted in this work is from Rajasekhara et al. (2017) and are shown in Table A1. The Zirlo clad was modeled using isotope concentration for each chemical element and their respective isotopic abundances which were obtained from Berglund and Wieser (2009).

Table A1
Zirlo composition (Rajasekhara et al., 2017).

Nuclide	Concentration (w/o)
Sn	0.48
Fe	0.11
Nb	1.01
Cr	0.01
Zr	Balance

The compositions of the UO_2 pellets were based on the different enrichments. For a typical fuel used by Westinghouse the ^{234}U content is given by (Godfrey, 2014)

$$W_{234} = 0.00731\ W_{235}^{1.0837} \tag{A1}$$

where W_{23x} is the enrichment of each given uranium isotope in weight %. The UO_2 specific mass was obtained from Walker (2014). Its value is compatible with the total mass of U present in the AP1000 core at BOC (Westinghouse, 2011).

The specific mass for the gap and water were obtained from Walker (2014). The gap and water compositions are based on natural isotopic abundance (Berglund and Wieser, 2009), the specific mass for the water at 300 K and 565 K are presented in Table A1 (Walker, 2014).

A2. Materials and geometric data for the IFBA burnable absorber rods

Fig. A3 shows a schematic of the Integral Fuel Burnable Absorber rod presenting dimensions and materials. The IFBA is a fuel pellet coated with a thin ZrB_2 neutron absorber cover. There is no much information about the exact dimensions of the fuel pellet and ZrB_2 cover thickness in the literature (Westinghouse, 2011). The ZrB_2 coating is considered 0.000508 cm thick according to the Walker (2014) IFBA model. Since the outer IFBA pellet radius is similar to that of the fuel pellet (see Fig. A1) the actual fuel content of the IFBA pellet is slightly smaller. Table A2 presents the materials data for the IFBA with their respective source.

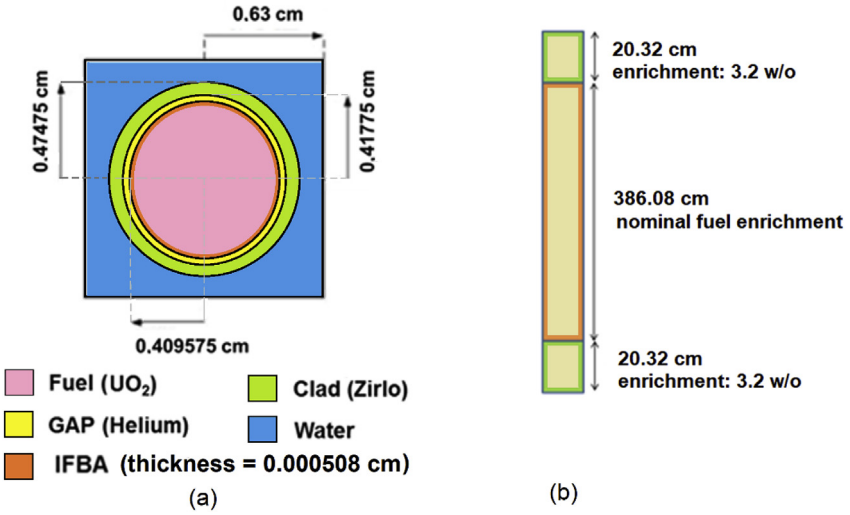

Fig. A3. Cross sections showing the dimensions of the IFBA burnable absorber rod including, gap, Zirlo clad, ZrB_2 coating, and axial ^{235}U enrichment.

Table A2
Materials data for the IFBA burnable. absorbers with their respective source.

Parameter	Value
^{10}B loading †	0.772 mg/cm
Absorber height †	386.08 cm
Material †	ZrB_2
ZrB_2 specific mass *	6.09 g/cm^3
^{10}B enrichment *	50%
ZrB_2 coating thickness ‡	5.08×10^{-4} cm

† (Westinghouse, 2011).
* (Walker, 2014).
‡ (Franceschini et al., 2014).

A3. Materials and geometric data for the Pyrex burnable absorber rods

The initial core of AP1000 uses Pyrex Burnable Absorber (borosilicate glass B_2O_3—SiO_2). The Pyrex burnable absorber composition data are presented with detail in the Vera reports (Godfrey, 2014). Fig. A4 presents a schematic of the Pyrex burnable absorber rod and its materials and geometric data are presented in Table A3. The original data from Godfrey (2014) related to the length of the rod were adapted to be compatible with that presented in Westinghouse (2011).

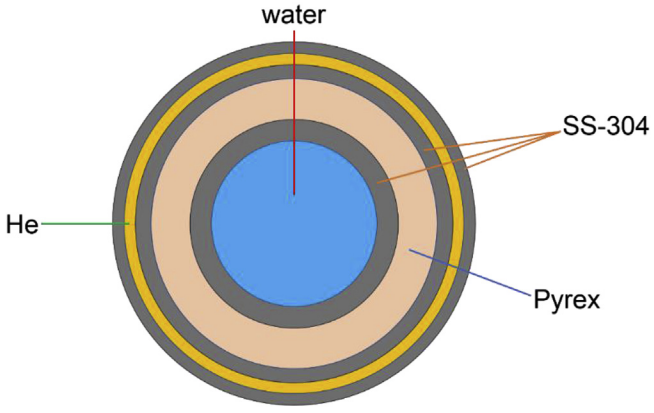

Fig. A4. Schematic of the Pyrex burnable absorbers rod.4

Table A3
Materials and geometric data for the Pyrex burnable. Absorber (Godfrey, 2014).

Input	Value
Neutron absorber material	B_2O_3—SiO_2 (borosilicate glass Pyrex)

(*continued on next page*)

Table A3 (*continued*)

Input	Value
Inner tube material	SS-304
Plenum material	Helium
Clad material	SS304
Boron-10 loading	6.24 mg/cm
Pyrex specific mass	2.23 g/cm^3
SS304 specific mass	8.00 g/cm^3
Inner tube inner radius	0.214 cm
Inner tube outer radius	0.231 cm
Pyrex inner radius	0.241 cm
Pyrex outer radius	0.427 cm
Clad inner radius	0.437 cm
Clad outer radius	0.484 cm
Absorber height	368.3 cm

Standard Pyrex contains traces of other compounds such as Na_2O, Al_2O_3, Fe_2O_3, CaO, MgO and Cl. These are ignored here because only compounds containing boron-10 will significantly affect the neutron absorption rate (Godfrey, 2014). The stainless steel (SS-304) composition is taken from typical Westinghouse reactors (Godfrey, 2014).

A4. Configuration of burnable absorber rods on the fuel assemblies

The configurations of burnable absorber rods are complex and shown in Figs. A5 and A6 for the IFBA and Pyrex types. Their disposition aims at providing adequate control of core reactivity throughout the first core (BOC). The configurations for the IFBA burnable absorber rods were obtained from Westinghouse (2011), and those for the Pyrex burnable absorber rods, from Ames et al. (2009). The number and disposition of the rods in the fuel assembly change for different configurations.

The Pyrex configurations with 12 and 9 burnable absorber rods are not symmetric. They can be positioned in the core with different orientations with impact in the core reactivity and neutron flux distribution. We assumed the arrangement shown in Fig. A7 in which the sides with fewer burnable absorber rods face the core center. This detail was not found in the reviewed literature.

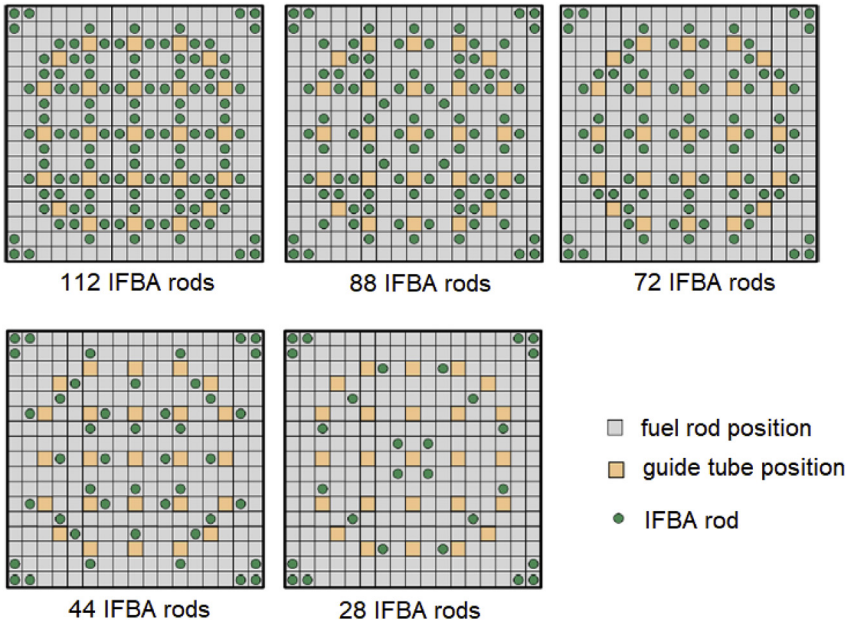

Fig. A5. Configurations for the IFBA burnable absorber rods in the AP1000 fuel assemblies (Westinghouse, 2011).5

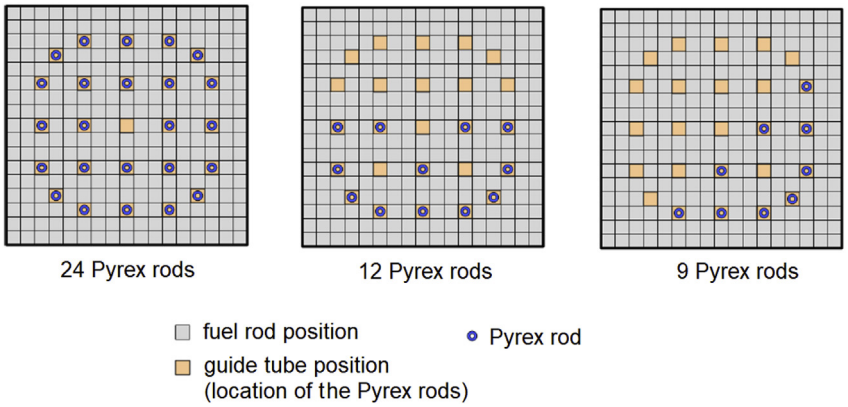

Fig. A6. Configurations for the Pyrex burnable absorber rods in the AP1000 fuel assemblies (Ames et al., 2009).6

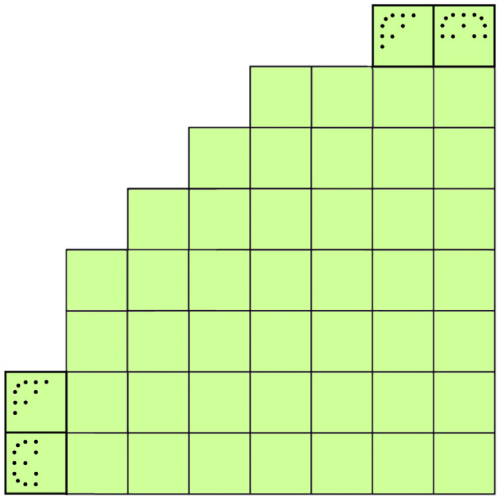

Fig. A7. Orientation in the core adopted in this work for the fuel assemblies with 9 and 12 Pyrex burnable absorbers.7

References

Alhaj, M.Y., Badawi, A., Abou-Gabal, H.H., Mohamed, N.M.A., 2016. Partial loading of thorium-plutonium fuel in a pressurized water reactor. Nucl. Technol. 194, 314–323.

Ames II, D.E., Tsvetkov, P.V., Rochau, G.E., Rodriguez, S., 2009. High-fidelity Nuclear Energy System Optimization towards an Environmentally Benign, Sustainable and Secure Energy Source. Albuquerque. Sandia Report SAND2009-6831. .

Baldova, D., Fridman, E., Shwageraus, E., 2014. High conversion Th–U233 fuel for current generation of PWRs: Part II – 3D full core analysis. Ann. Nucl. Energy 73, 560–566.

Bell, G.I., Glasstone, S., 1970. Nuclear Reactor Theory, Chapt. 6. Van Nostrand Reinhold, New York pag. 273.

Berglund, M., Wieser, M.E., 2009. Isotopic compositions of the elements 2009 (IUPAC technical report). Pure Appl. Chem. 83, 397–410.

Chambers, A., Ragusa, J.C., 2014. Multi-recycling of transuranic elements in a PWR assembly with reduced fuel rod diameter. Nucl. Eng. Des. 270, 436–450.

Elsawi, M.A., Hraiz, A.S.B., 2015. Benchmarking of the WIMS9/PARCS/TRACE code system for neutronic calculations of the Westinghouse AP1000 reactor. Ann. Nucl. Energy 293, 249–257.

Ernout, M., David, S., Doligez, X., Meplan, O., Leniau, B., Bidaud, A., Nuttin, A., Mouginot, B., Wilson, J., Capellan, N., Thiolliere, N., 2015. Advanced plutonium management in PWR, complementarity of thorium and uranium. Prog. Nucl. Energy 78, 330–340.

Franceschini, F., Godfrey, A., Kulesza, J., Oelrich, R., 2014. Westinghouse VERA Test Stand - Zero Power Physics Test Simulations for the AP1000 PWR. CASL Technical Report CASL-U-2014-0012-001.

Franceschini, F., Godfrey, A.T., Stimpson, S., Evans, T., Collins, B., Gehin, J.C., Turner, J., Graham, A., Downar, T., 2015. AP1000 PWR Startup Core Modeling and Simulation with VERA-CS. Advances in Nuclear Fuel Management V, Hilton Head Island, South Carolina, USA, March 29 – April 1, 2015. American Nuclear Society.

Godfrey, A.T., 2014. VERA Core Physics Benchmark Progression Problem Specifications. Technical Report CASL-U-2012-0131-004. CASL.

Huwaldt, J. A., Plot Digitizer 2.6.8. In: https://sourceforge.net/projects/plotdigitizer/files/plotdigitizer/2.6.8/. Accessed in 10/27/2015.

Kerby, L., Tumulak, A., Leppänen, J., Valtavirtaz, V., 2017. Preliminary serpent–MOOSE coupling and implementation of functional expansion tallies in serpent. In: International Conference on Mathematics & Computational Methods Applied to Nuclear Science & Engineering, Jeju, Korea, April 16-20.

Leppanen, J., June 18, 2015. Serpent - a Continuous-Energy Monte Carlo Reactor Physics Burnup Calculation Code - User's Manual. http://montecarlo.vtt.fi/.

Leppanen, J., Pusa, M., Viitanen, T., Valtavirta, V., Kaltiaisenaho, T., 2015. The Serpent Monte Carlo code: status, development and applications in 2013. Ann. Nucl. Energy 82, 142–150.

Lindley, B.A., Franceschini, F., Parks, G.T., 2014. The closed thorium–transuranic fuel cycle in reduced-moderation PWRs and BWRs. Ann. Nucl. Energy 63, 241–254.

Maiorino, J.R., Stefani, G.L., Moreira, J.M.L., Rossi, P.C.R., Santos, T.A., 2017. Feasibility to convert an advanced PWR from UO2 to a mixed U/ThO2 core – Part I: parametric studies. Ann. Nucl. Energy 102, 47–55.

Moreira, J.M.L., Cesaretti, M.A., Carajilescov, P., Maiorino, J.R., 2015. Sustainability deterioration of electricity generation in Brazil. Energy Policy 87, 334–346.

Moreira, J.M.L., Gallinaro, B., Carajilescov, P., 2013. Construction time of PWRs. Energy Policy 55, 531–542.

NEA, 2006. Advanced Nuclear Fuel Cycles and Radioactive Waste Management. NEA no 5990. Nuclear Energy Agency (Organisation for Economic Cooperation and Development).

Palmtag, S., Godfrey, A.T., 2014. VERA Common Input User Manual, CASL Technical Report CASL-U-2014-0014-002.

Rajasekhara, S., Kotula, P.G., Enos, D.G., Doyle, B.L., Clark, B.G., 2017. Influence of Zircaloy cladding composition on hydride formation during aqueous hydrogen charging. J. Nucl. Mater. 489, 222–228.

Souza, R.M.G.P., Moreira, J.M.L., 2006. Neural network correlation for power peak factor estimation. Ann. Nucl. Energy 33, 594–608.

Souza, R.M.G.P., Moreira, J.M.L., 2006a. Power peak factor for protection systems – experimental data for developing a correlation. Ann. Nucl. Energy 33, 609–621.

Stefani, G.L., 2017. Sobre a validade de conversão de um reator avançado PWR com núcleo de UO_2 para $(Th,U)O_2$. Ph.D. Thesis. Universidade Federal do ABC, Santo André.

Viitanen, T., Leppänen, J., 2012. Explicit treatment of thermal motion in continuous-energy Monte Carlo tracking routines. Nucl. Sci. Eng. 171, 165–173.

Walker, D.E., 2014. Modeling Integral Fuel Burnable Absorbers Using the Method of Characteristics. Master Thesis. The University of Tennessee, Knoxville.

Westinghouse, Westinghouse, 2011. AP1000 Design Control Document Rev. 19. Section 4.3 – Reactor, Nuclear Design. https://www.nrc.gov/docs/ML1117/ML11171A445.pdf.